Ab Initio Spectroscopy of Natural and Artificial Fire Contaminants for Microwave Frequency (V/W Band) Signal Absorbance

THESIS

Matthew B. Husk

AFIT-ENG-MS-18-D-001

DEPARTMENT OF THE AIR FORCE
AIR UNIVERSITY

AIR FORCE INSTITUTE OF TECHNOLOGY

Wright-Patterson Air Force Base, Ohio

AFIT-ENG-MS-18-D-001

AB INITIO SPECTROSCOPY OF NATURAL AND ARTIFICIAL FIRE CONTAMINANTS FOR MICROWAVE FREQUENCY (V/W BAND) SIGNAL ABSORBANCE

THESIS

Presented to the Faculty

Department of Engineering Physics

Graduate School of Engineering and Management

Air Force Institute of Technology

Air University

Air Education and Training Command

in Partial Fulfillment of the Requirements for the

Degree of Master of Science in Applied Physics

Matthew B. Husk, B.S.

March 2021

AFIT-ENG-MS-18-D-001

AB INITIO SPECTROSCOPY OF NATURAL AND ARTIFICIAL FIRE CONTAMINANTS FOR MICROWAVE FREQUENCY (V/W BAND) SIGNAL ABSORBANCE

THESIS

Matthew B. Husk, B.S.

Committee Membership:

Larry Burggraf, Ph.D.
Advisor

Frank Duan, Ph.D.
Advisor

Steven Fiorino, Ph.D.
Committee

Andrew Terzuoli, Ph.D.
Committee

AFIT-ENG-MS-18-D-001

Abstract

The rotation and vibration spectral properties including frequencies and intensities for highly concentrated molecules present in wildland and artificial fires have been studied. Properties were used to determine absorption and its effect in a link budget analysis. Absorption in link budget analyses is commonly accounted for via line-by-line methodology aided by HITRAN documented intensities. Limited, if any, customization of spectral properties is available with HITRAN and other spectral databases. *Ab initio* quantum chemistry calculations with Dunning's correlation consistent triple and quadruple-zeta atomic basis sets were employed to obtain structures, dipole moments, rotational-vibrational frequencies and intensities, as well as various coupling parameters. Anharmonic corrections to the vibrational energies are included in the calculations. The values of these parameters were found to be in agreement with experimental data while allowing flexibility for the inclusion or exclusion of spectral properties for various gases. Discussed here is molecular absorption in relation to a link budget, an overview of vibration-rotation constants for various molecular geometries, a description of intensities calculated from transition dipole, and lastly power-loss due to absorption.

Acknowledgements

This work was made possible thanks to our sponsor

Air Force Research Laboratory/RIT

Paul F. Gilgallon, Principal Engineer, NC3 Systems and Technology Lead

525 Brooks Road

Rome, NY 13441.

I would also like to thank my committee for all their help in constructing this work.

Special thanks to Dr. Frank Duan.

Special thanks to Joe Sugrue.

Matthew B. Husk

Table of Contents

Page

List of Figures

List of Tables

AB INITIO SPECTROSCOPY OF NATURAL AND ARTIFICIAL FIRE CONTAMINANTS FOR MICROWAVE FREQUENCY (V/W BAND) SIGNAL ABSORBANCE

I. Introduction

1.1 Background and Motivation

The use of radio wave frequencies for communications is, in general, favored due to their inherently long wavelengths and wide variety of applications. As outlined by the International Telecommunication Union (ITU), the spectrum of radio frequencies are divided into bands ranging from 3 Hz (10^5 km) to upwards of 3 THz (0.1 mm) [1]. Of interest to us are the Institute of Electrical and Electronics Engineers (IEEE) radar bands, 10 groups spanning 1-300 GHz and assigned a letter denomination [2]. Frequencies within this band are referred to as microwave and provide services ranging from television broadcast, cellular communication, remote sensing, communications satellite, and numerous others. The advantages of communications satellites, or SATCOM, can be attributed to large frequency bandwidth and nearly global communication ranges. Higher frequency SATCOM bands provide benefits such as high-speed data transfer, increased remote sensing capabilities, and high resolution radio astronomy. Unfortunately, issues arise at these higher frequencies as well, where significant atmospheric attenuation from gaseous absorption creates issues for long distance signal path lengths.

Molecules associated with naturally occurring forest fires, and artificial fires from High Altitude Nuclear Explosions (HANES), can interfere with RF signal and atten-

uate the V (40-75 GHz) and W (75-110 GHz) frequency bands [3]. As a result, the molecular absorption spectra of molecules arising from these events are of interest. This research will determine spectroscopic properties of these molecules in order to predict atmospheric attenuation from gaseous absorption of satellite communications in the unfavorable conditions of natural and artificial fire emissions.

1.2 Problem Statement

Current models for propagation of signals at the V/W frequency bands lack accurate predictions of atmospheric attenuation and are still in development [3]. The potential for plumes due to natural or artificial fire from HANES poses a risk for signal attenuation and signal loss [4]. Chemical composition measurements have been conducted for wild-land fire emissions [5][6]. High temperatures associated with these plumes have a thermal broadening effect, increasing particle velocity and giving rise to wider spectral lines of molecules which reside in the plume. Due to the extreme nature of these large scale phenomena it is difficult to accurately experimentally measure effects these molecules contribute to signal attenuation. This creates a need for experimentally-validated theoretical models, capable of simulating these harsh environments to predict the impact of these molecules. The discussed atmospheric attenuation modeling will provide support; for satellite link budget analyses and developing future V/W band SATCOM capabilities, and for modeling gas compositions for which experimental spectroscopy has not been measured.

1.2.1 Specific Problem

The Robust Aerial Pathways for Nuclear Command, Control and Communication (NCCC or NC3) supports research into the modeling of scintillation and attenuation due to atmospheric phenomena and contamination by particulate matter in the V

and W bands [7]. There is a lack of adequate models capable of accurately predicting signal performance at these bands. Development of attenuation models is needed to develop an understanding of SATCOM communications of natural and artificial environments. The key deliverable is a preliminary attenuation model for satellite link budget analyses.

1.3 Research Objective, Questions, Hypotheses, Focus

Rotational motion of small molecules generated by fires, such as hydrogen cyanide (HCN) and carbon monoxide (CO) can produce absorption in V and W bands. Rovibrational motion can absorb in microwave and with some specific instances, such as HCN vibrational bending modes with high rotational J values, in the V and W bands. Molecular absorption in Laser Environmental Effects and Definition and Reference (LEEDR) [8] relies on line intensity information from the High-Resolution Transmission (HITRAN) database [9]. The HITRAN database is a collection of experimental and theoretically calculated spectroscopic parameters for a variety of molecules [10]. While extremely helpful, HITRAN does not have data on every single molecule nor does it always include every spectroscopic parameter for a transition. As the HITRAN database is only updated every 4 years, a method for determining line intensities which are not fully present in HITRAN is of interest. We would like to know if a method for *ab initio* calculation of line intensities can be implemented into LEEDR for molecules which can be described as asymmetric top, symmetric top, linear polyatomic, and diatomic. If the *ab initio* line intensities are in agreement with literature values and the methodology is not overly complex, implementation of the method into LEEDR can provide reasonably accurate absorbance values for molecules which have not been looked at due to lack of data. This paper intends to focus on high precision and accuracy for *ab initio* calculated spectroscopic properties for molecules in which

a high atmospheric concentration was found as a result of natural and artificial fires. A simplistic plume diffusion model is included to aid in approximating a link budget calculation for V/W bands.

1.4 Approach/Method

This is a study of the geometry, ro-vibrational, and rotational spectrum of molecules that may influence propagation in the V/W frequency bands. The first step is to identify and select the molecules which have ro-vibrational and/or rotational frequencies within or near the V/ W bands. Molecular Orbital Theory (MO Theory) and Density Functional Theory (DFT) calculations are employed to predict the physical properties of the molecules relevant to their spectroscopy. Spectroscopic parameters of optimized molecular structures are used to predict and simulate the transmission and emission of light in the atmosphere. Hitran and NASA Jet Propulsion Laboratory (JPL) describe many molecules that absorb in our area of interest, the 40-75 GHz (1.34-2.50 cm^{-1}) V and 75-110 GHz (2.50-3.67 cm^{-1}) W frequency bands. For molecules whose spectroscopy is not measured, we use the computational chemistry software, Gaussian [10], to optimize the molecular geometries and predict their physical properties. Changes in attenuation as a result of spectral intensities are also predicted.

1.5 Assumptions/Limitations

This research assumes molecules are individual constituents of a singular isotopologue abundance. If mixing of isotopologues is desired, a separate calculation must be carried out. There are instances where Gaussian is not capable of calculating certain spectroscopic parameters for a molecule. In these cases it is assumed the formulas for spectroscopic constants obtained by low-order perturbation theory have acceptable error and do not break down at large values. It is assumed variations in constants

for the basis sets are reasonably small. For the case of modeling plume dispersion, a non-physical worst case situation is assumed in order to provide a simple method for approximating the link budget.

This research is limited to the linear polyatomic molecule $H^{12}C^{14}N$. It is assumed HCN is found in both natural and artificial fires. Single transitions from both rotational states and the ground vibrational state to first excited state are considered. The current state of this research does not include electronic excited-state transitions or combination bands. The vibrational bending modes of HCN are also neglected at this time.

1.6 Implications

This research offers a possible supplementation to LEEDR's molecular absorption capabilities. By providing the opportunity of an *ab initio* approach, users can have the freedom to customize their molecule's physical parameters without the limitation of only using HITRAN available data. An initial molecular attenuation model is also provided to help predict signal performance at V/W bands.

1.7 Preview

This paper begins with Chapter II: Literature Review, which discusses history of radio frequency bands with their applications, previous molecular absorption studies, and a review of gas constituents from fires. Following this is Chapter III: Theoretical Background, providing a background for spectroscopic constants in vibration-rotation interaction, spectral line intensities, spectral line shape functions, absorbance, and attenuation. In Chapter IV: Methodology, an explanation of the overall process is given for *ab initio* spectroscopy calculations and the plume dispersion model. Chapter V: Results and Analysis, we compare our calculations to experimentally accepted

values for spectroscopic parameters and line intensities. The P and R branches are also shown here. The plume dispersion model is then presented along with the attenuation calculation for our modeled HCN plume. In Chapter VI: Discussion, a relevance of this work is given followed by an outline for future work.

II. Literature Review

2.1 History of SATCOM and V/W Bands

Satellite Communication (SATCOM) can be defined as communications channel utilizing an artificial space-based satellite and a terrestrial receiver. Implementation of SATCOM increases global telecommunication by greatly reducing the restriction from line-of-sight links. Alternate methods for beyond the horizon telecommunication include sky-wave and surface-wave propagation. Issues arise with these methods in the HF (High Frequency, 3-30 MHz) band and become more pronounced beyond 30 MHz. There is a push for SATCOM system development into higher frequency sub-bands in the EHF (Extremely High Frequency, 30-300 GHz) band, in particular the V (40-75 GHz) and W (75-110 GHz) bands [3]. Current systems belong to the SHF (Super High Frequency, 3-30 GHz) band, and favor the C (4-8 GHz), X (8-12 GHz), Ku (12-18 GHz), and Ka (26.5-40 GHz) bands due to increased bandwidth availability above the crowded UHF (0.3-3 GHz) bands [11]. The benefits of V/W frequency band utilization have long been known, offering an enticing array of applications coupled with high-speed multi-gigabit data transfer.

III. Theoretical Background

3.1 Link Budget

The success or failure of a radio frequency (RF) telecommunications link can be summarized with a link budget. Beginning at the transmitter of the system, there is a power output which is regarding as the initial power of an RF link. The path traveled by a signal from transmitter to receiver is defined as the total signal path. Signal gains and losses may occur between transmitter and receiver are quantified. Beginning with the output power of the transmitter and including all signal gains and losses, one is left with the expected power delivered to the receiver. It is generally accepted that having a value greater than unity for the transmitter-receiver ratio is a good idea. A standard link budget equation [12]

$$P_r = P_t - L_t - L_r - L_{path} + G_t + G_r, \tag{1}$$

is expressed in terms of dBm (decibel-milliwatt) and the terms are as follows: P_r power at receiver, P_t power at transmitter, L_t loss at transmitter, L_r loss at receiver, L_{path} loss from path between transmitter and receiver antennas, G_t gain from transmitter, G_r gain from receiver.

3.2 Attenuation and Beer-Lambert Law

Attenuation, or extinction, is a contributor to path loss and occurs when there is reduction in amplitude of the signal in a medium. The inclusion of the Beer-Lambert law explains the relationship between signal attenuation and medium of travel. Beginning with a first-order linear differential equation [13]

$$\frac{d\Phi_e(z)}{dz} = \mu(z)\Phi_e(z), \tag{2}$$

where $\Phi_e(z)$ denotes emitted radiant flux, $\mu(z)$ the attenuation coefficient, and z as altitude. Using the method of an integrating factor and some simplifying of terms, an equation for radiant flux propagating through a material of thickness z is given [13]

$$\Phi_e^t = \Phi_e^i e^{-\int_0^z \mu(z'),dz'}, \tag{3}$$

where the dependence on z is now explicitly dependent on only the attenuation coefficient. Equation 3.3 is useful as it is a good starting point for deriving unique relations, such as transmittance T [13]

$$T = \frac{\Phi_e^t}{\Phi_e^i} = e^{-\int_0^z \mu(z')dz'}, \tag{4}$$

where $\mu(z)$ represents the attenuation coefficient comprising the absorption and scattering coefficients, $\mu = \mu_a + \mu_s$. The above transmittance equation is then related to the absorbance as [13]

$$A = -\log_{10} T, \tag{5}$$

While the above equations are able to approximate absorption, it excludes concentration of states and stimulated emission.

3.3 Vibration-Rotation Interaction: Asymmetric Tops

Molecules have three main types of motion capable to absorb energy from communication signals: vibrational, rotational, and translational. Historically, term values have been used to represent the energy expressions associated with each motion. Term values represent energy eigenvalues of the corresponding Hamiltonian operator. In this paper we are considering vibration-rotation interaction and therefore use the vibration-rotation term value, comprising the summation of vibrational and rotational term values [14]

$$T(v, J) = G(v) + F_v(J). \tag{6}$$

3.3.1 Energy Expressions

The vibrational term values, $G(v)$, for an asymmetric top are expressed as [14]

$$G(v) = \sum_r \omega_r (v_r + \frac{1}{2}) + \sum_{r \geq s} \chi_{rs} (v_r + \frac{1}{2})(v_s + \frac{1}{2}) + ..., \tag{7}$$

where ω is a harmonic vibrational frequency, χ a vibrational anharmonic constant, and v represents the vibrational quantum number. The rotational term values, $F_v(J)$, are a bit more involved than their vibrational counterpart and require the eigenvalues of an effective reduced rotational Hamiltonian of the form [14]

$$\frac{\tilde{H}_{rot}}{hc} = \sum_\alpha \tilde{B}_v^{(\alpha)} J_\alpha^2 - \Delta_J J^4 - \Delta_{JK} J^2 J_z^2 - \Delta_K J_z^4 - 2\delta_J J^2 (J_x^2 - J_y^2)$$

$$\text{-}\delta_K [J_z^2 (J_x^2 - J_y^2) + (J_x^2 - J_y^2) J_z^2] + H_J J^6 + H_{JK} J^4 J_z^2 + H_{KJ} J^2 J_z^4$$

$$+ H_k J_z^6 + 2h_J J^4 (J_x^2 - J_y^2) + h_{JK} J^2 [J_z^2 (J_x^2 - J_y^2) + (J_x^2 - J_y^2) J_z^2]$$

$$+ h_k [J_z^4 (J_x^2 - J_y^2) + (J_x^2 - J_y^2) J_z^4] + ...(8)$$

3.4 Vibration-Rotation Interaction: Symmetric Tops

3.4.1 Energy Expressions

The vibrational term values, $G(v)$, for an asymmetric top are expressed as [15]

$$G(v) = \sum_r \omega_r(v_r + \frac{1}{2}d_r) + \sum_{r \geq r'} \chi_{rr'}(v_r + \frac{1}{2}d_r)(v_r^{'} + \frac{1}{2}d_s) + \sum_{t \geq t'} g_{tt'} l_t l_{t'} + ... \qquad (9)$$

where ω is a harmonic vibrational frequency, χ a vibrational anharmonic constant, and v represents the vibrational quantum number. The rotational term values, $F_v(J)$, are of the form [15]

$$F_v(J) = B_v[J(J+1) - K^2] + A_v K^2 - \sum_t 2(A\zeta_t)_v k l_t$$

$$\text{-D}_{Jv}[J(J+1)]^2 - (D_{JK})_v J(J+1)K^2 - (D_K)_v K^4$$

$$+ \textstyle\sum_t (n_{tJ})_v J(J+1) k l_t + \sum_t (n_{tk})_v k^3 l_t + ...(10)$$

3.5 Vibration-Rotation Interaction: Linear Polyatomic

3.5.1 Energy Expressions

The vibrational and rotational term values are much less involved for a linear polyatomic molecule. Rotational term values $F_v(J)$ have vibrational dependence and are expressed as [16]

$$F_v(J) = B_v[J(J+1) - l^2] - D_J[J(J+1) - l^2]^2 + H_J[J(J+1) - l^2]^3 + ... \qquad (11)$$

where quantum number l is total angular momentum due to vibrational effects, B_v is the vibrationally dependent effective rotational constant, D_J the quartic centrifugal distortion constant, and H_J the sextic centrifugal distortion constant.

Vibrational term values do not have a rotational dependence and are expressed as [16]

$$G(v) = \sum_r \omega_r(v_r + \frac{1}{2}d_r) + \sum_{r \geq s} \chi_{rs}(v_r + \frac{1}{2}d_r)(v_s + \frac{1}{2}d_s) + \sum_{t \geq t'} g_{tt'} l_t l_{t'} + ... \qquad (12)$$

where r indicates any vibrational mode, s a non-degenerate mode, and t a degenerate mode. The ω_r represents harmonic frequency of the rth vibrational mode, v_r is the fundamental mode, d is the degeneracy, χ_{rs} and $g_{l_t l_{t'}}$ are the diagonal and off-diagonal vibrational anharmonic constants.

3.5.2 Vibration-Rotation Interaction Constants

As discussed above in Eq.(11), rotational term values have a vibrational dependence. These vibrational dependencies are generally hidden in the effective constants preceding each bracketed expression. In our case, we have opted to only account for vibrational dependence in the first constant, B_v [17]

$$B_v = B_e - \sum_r \alpha_r(v_r + \frac{1}{2}d_r) \qquad (13)$$

where $B_e = \frac{h^2}{8\pi^2 I_e}$ represents the equilibrium rotational constant in which no net torque is acting on the molecule, and α_r is an interaction constant giving the first-order correction of B_v. This interaction constant, sometimes called the vibration-rotation interaction constant, can be derived from low-order perturbation theory for non-degenerate [16]

$$\alpha_s = -\frac{2B_e^2}{\omega_s}[\frac{3a_s^2}{4I_e} + \sum_t \zeta_{st}^2 \frac{3\omega_s^2 + \omega_t^2}{\omega_s^2 - \omega_t^2} + \pi(\frac{c}{h})^{1/2} + \sum_{s'} \phi_{sss'} a_{s'} \frac{\omega_s}{\omega_s^{3/2}}] \tag{14}$$

and degenerate [16]

$$\alpha_t = -\frac{2B_e^2}{\omega_t}[\frac{1}{2}\sum_s \zeta_{st}^2 \frac{3\omega_t^2 + \omega_s^2}{\omega_t^2 - \omega_s^2} + \pi(\frac{c}{h}^{1/2}) \sum_s \phi_{stt} a_s \frac{\omega_t}{\omega_s^{3/2}}] \tag{15}$$

modes. In Eqs. (14) and (15), $a_s = \frac{\partial I_e}{\partial Q_r}$ is the moment of inertia derivative with respect to a normal mode Q_r, $I_e = \mu r_e^2$ the equilibrium moment of inertia with nuclei separation r_e and an effective reduced mass μ, ζ the Coriolis coupling, and ϕ_{rrr} the cubic force constant in normal modes.

3.5.3 Centrifugal Distortion Constants

The centrifugal distortion constants used in this paper are the quartic, D_J, and sextic H_J terms. These constants share a similarity to B_e, in which they account for first and second-order centrifugal distortion effects due to the rotation of a molecule about its equilibrium moment of inertia. As previously mentioned, the terms preceding the second and third brackets in Eq.(11) can be written in terms of an effective distortion constant [17]: $D_v = D_e + \beta_e(v + \frac{1}{2}) + ...$ and $H_v = H_e + \gamma_e(v + \frac{1}{2}) + ...$, where $D_e = D_J$ and $H_e = H_J$. This accounts for the effect vibration has on centrifugal distortion of a rotating molecule. For the purposes of this paper, vibrational contribution to rotational constants are only included up to B_v and we can represent the quartic centrifugal distortion constant, D_J, as [16]

$$D_J = \frac{1}{2}\sum_s \frac{B_s^2}{\omega_s} \tag{16}$$

and the sextic centrifugal distortion constant, H_J, as [16]

$$H_J = \frac{4D_J^2}{B_e} - 2B_e^2 \sum_s \frac{B_s^2}{\omega_s^3} - \frac{1}{6} \sum_{ss's''} \phi_{ss's''} \frac{B_s B_{s'} B_{s''}}{\omega_s \omega_{s'} \omega_{s''}}. \quad (17)$$

In the above equations we have used the definition of a rotational derivative, B_s, to describe the distortion constants [16]

$$B_s = -\frac{\hbar^3}{2h^{3/2}c^{3/2}\omega^{1/2}} \frac{a_s}{I_e^2}. \quad (18)$$

3.5.4 Vibrational Anharmonic Constants

Vibrational anharmonic constants arise from the splitting of the vibrational angular momentum, l, as a result of anharmonic vibrations. The equations for these constants are [16]

$$\chi_{ss} = \frac{1}{16}\phi_{ssss} - \frac{1}{16} \sum_{s'} \phi_{sss'}^2 \frac{8\omega_s^2 - 3\omega_{s'}^2}{\omega_{s'}(4\omega_s^2 - \omega_{s'}^2)}, \quad (19)$$

$$\chi_{tt} = \frac{1}{16}\phi_{tttt} - \frac{1}{16} \sum_{s} \phi_{stt}^2 \frac{8\omega_t^2 - 3\omega_s^2}{\omega_s(4\omega_t^2 - \omega_s^2)}, \quad (20)$$

$$\chi_{l_t l_t} = \frac{1}{48}\phi_{tttt} - \frac{1}{16} \sum_{s} \phi_{stt}^2 \frac{\omega_s}{4\omega_t - \omega_s^2)}, \quad (21)$$

$$\chi_{ss'} = \frac{1}{4}\phi_{sss's'} - \frac{1}{4} \sum_{s''} \phi_{sss''}\phi s''s'\frac{1}{\omega s''} - \frac{1}{2} \sum_{s''} \phi_{ss's''}^2 \frac{\omega_s(\omega_{s''}^2 - \omega_s^2 - \omega_{s'}^2)}{\Delta_{ss's''}}, \quad (22)$$

$$\chi_{st} = \frac{1}{4}\phi_{sstt} - \frac{1}{4} \sum_{s'} \phi_{sss'}\phi s'tt\frac{1}{\omega s'} - \frac{1}{2} \sum_{t'} \phi_{stt'}^2 \frac{\omega_{t'}(\omega_{t'}^2 - \omega_s^2 - \omega_t^2)}{\Delta_{stt'}} + B_e\zeta_{st}^2(\frac{\omega_s}{\omega_t} + \frac{\omega_t}{\omega_s}), \quad (23)$$

$$\chi_{tt'} = \frac{1}{8}(\phi_{t_a t_a t_{a'} t_{a'}} + \phi_{t_a t_a t_{b'} t_{b'}}) - \frac{1}{4}\sum_s \phi_{stt}\phi st't' \frac{1}{\omega s} - \frac{1}{4}\sum_s \phi^2_{stt'} \frac{\omega_s(\omega_s^2 - \omega_t^2 - \omega_{t'}^2)}{\Delta_{stt'}} + B_e \zeta^2_{st}(\frac{\omega_s}{\omega_t} + \frac{\omega_t}{\omega_s}), \tag{24}$$

and

$$\chi_{l_t l_{t'}} = \frac{1}{2}\sum_s \phi^2_{stt'} \frac{\omega_s \omega_t \omega_{t'}}{\Delta_{stt'}} \tag{25}$$

in which the term $\Delta_{rr'r''} = (\omega_r + \omega_{r'} + \omega_{r''})(\omega_r + \omega_{r'} - \omega_{r''})(\omega_r - \omega_{r'} + \omega_{r''})(\omega_r - \omega_{r'} - \omega_{r''})$ represents the possible combinations of harmonic frequencies ω_r [16]. The ϕ_{rrrr} terms are the quartic force constants.

3.5.5 Fundamental Frequencies

Frequencies resulting from the vibrational ground state $v = 0$ to first excited state $v = 1$ transition are referred to as fundmental. For a linear polyatomic molecule, these frequencies are given as [16]

$$\nu_i = \omega_i + \chi_{ii}(1 + d_i) + \frac{1}{2}\sum_{k \neq i} \chi_{ik} d_k + \chi_{lili}. \tag{26}$$

From this, we can see how the fundamental frequencies arise from a combination of the harmonic frequencies and anharmonic constants with their corresponding degeneracies.

3.6 Stimulated Emission

3.6.1 Total Power and Beer-Lambert

Referring back to Eqn.(3), the Beer-Lambert law with the inclusion of state concentrations and stimulated emission is represented by the following [18]

$$\Phi = \Phi_o e^{-\sigma(N_o - N_1 \frac{2J"+1}{2J'+1})l} = \Phi_o e^{-\alpha l}, \tag{27}$$

in which N_1 and N_o denote the upper and lower state population of a single transition. With some variable substitutions and the assumption of thermodynamic equilibrium, a more useful Beer-Lambert law is given [18]

$$-ln(\frac{\Phi}{\Phi_o}) = \frac{\sigma(2J"+1)}{q} e^{\frac{-E_o}{kT}} (1 - e^{\frac{-h\nu_{10}}{kT}}) Nl, \tag{28}$$

in which σ is the cross section, q the partition function, J a rotational transition, k Boltzmann constant, T temperature in Kelvin, E_o the lower state energy, and ν_{10} the line frequency associated with a single transition.

3.7 Line Intensities

In this paper the term intensity refers to spectral irradiance given as $I = \int I_\nu d\nu$. The intensity of a rovibrational (rotational-vibrational) line at temperature T is calculated as [18]

$$S_{vr} = \frac{8\pi^3 \tilde{\nu}_{fi}}{3hc} \frac{L e^{\frac{-E_i}{kT}}}{Q_{vr}(T)} \frac{T_o}{T} (1 - e^{-\frac{E_f - Ei}{kT}}) S_{J'J"}, \tag{29}$$

in which the subscript on our line intensity and partition function to indicate rovibrational terms. E_i and E_f denote energy of the corresponding state, $\tilde{\nu}_{fi}$ the band center or transition wavenumber, $Q_{vr}(T)$ the rovibrational partition function as a

function of temperature T, and $S_{J'J''}$ the line strength. The constant L refers to the Loschmidt constant, the number of molecules per unit volume at 1 atm. For line intensity in terms of $cm^{-2}atm^{-1}$, the Loschmidt constant is given as $L = 2.68675\text{x}10^{19}$ $molecules\ cm^{-3}atm^{-1}$. It should be mentioned here, that T_o=273.15K and T is the user-specified temperature. The term $S_{J'J''}$ is called line strength and is defined as [18]

$$S_{J'J''} = |\mathbf{M}_{v'v''}|^2 S_{J''}^{\Delta J} F(m), \tag{30}$$

where $\mathbf{M}_{v'v''}$ is the purely vibrational line transition dipole given as [18]

$$\mathbf{M}_{v'v''} = \langle \psi_{v'} | \mu | \psi_{v''} \rangle, \tag{31}$$

and $S_{J''}^{\Delta J}$ the Hönl-London factor [18]

$$\sum_{\Delta J} S_{J''}^{\Delta J} = 2J'' + 1, \tag{32}$$

which is an expression for rotational line intensity in a transition relative to $J'' = 0$.

$F(m)$ is a correction term referred to as the Herman-Wallis factor. Although this term is neglected in our calculations, it is useful for precise applications. Herman-Wallis factors correct the error in separating the vibrational and rotational terms as was done in Eqn.(30). Specifically, the Herman-Wallis factors describe the effects of vibration-rotation interaction on the matrix elements of dipole moments. The dipole moment, or transition dipole, depends on total angular momentum *and* vibrational operators.

3.8 Plume Attenuation

In order to determine the attenuation from hydrogen cyanide in a link budget we need to model a fire plume.

3.8.1 Lorenztian Line Shape

Our spectral lines of hydrogen cyanide are fitted to the Lorentzian line shape function [19]

$$L = \frac{1}{1 + x^2} \tag{33}$$

where the variable x represents

$$x = \frac{p - p_o}{\omega/2} \tag{34}$$

with p being a position, p_o the position of the transition energy, and ω the full-width half-maximum.

3.8.2 Absorption Coefficient

Application will be applied to HCN molecules for illustration of this approach. The absorption coefficient represents the ease of HCN molecules traveling through a medium and can be represented by [9]

$$k_{ij}(\nu, T) = S_{ij}(T)L(\nu; \nu_{ij}, T) \tag{35}$$

where the spectral line intensities are indicated by S in $cm/molecule$ while the line shape function is L in units cm.

3.8.3 Column Number Density

Column number density, or absorbance, is a measure of the amount of matter between an initial and final location. The column number density of absorbing molecules is comprised of two factors and can be expressed as [9]

$$u = \int_z C(x, y, dz; H)dz \tag{36}$$

where the integral is over the altitude given as z. The concentration of the plume in gm^{-3} can be modeled by the general equation for a plume with reflection at plume height H given as [20]

$$C(x, y, z; H) = \frac{Q}{2\pi u \sigma_y \sigma_z} e^{\frac{-y^2}{2\sigma_y^2}} (e^{\frac{-(z-H)^2}{2\sigma_z^2}} + e^{\frac{-(z+H)^2}{2\sigma_z^2}}) \tag{37}$$

where Q is emission source strength in gs^{-1}, σ_y the horizontal width of the plume at any point downstream, σ_z the vertical extent of the plume at any position downstream, u wind speed ms^{-1}, and y and z represent the horizontal and vertical dispersion lengths, respectively.

3.8.4 Optical Depth

The dimensionless quantity optical depth measures the logarithmic ratio of incident and transmitted power through the plume in question and is given as [9]

$$\tau_{ij}(\nu, T) = u k_{ij}(\nu, T) \tag{38}$$

and is related to attenuation by [13]

$$\tau = ln(\frac{\Phi e^i}{\Phi_e^t}) = Aln(10) \tag{39}$$

where A is attenuation.

3.8.5 Attenuation

Attenuation can be expressed in terms of decibels dB and is written as [21]

$$A_{dB} = 10ln(e)\tau = 4.343\tau \tag{40}$$

where $10ln(e)$ is replaced with the attenuation coefficient 4.343.

IV. Methodology

4.1 Computational

4.1.1 Gaussian 16

The Gaussian 16 Quantum Chemistry Package was used to perform calculations for the spectroscopic parameters [10].

4.1.2 Functionals and Basis sets

For Hartree-Fock the Dunning's correlation-consistent basis sets were used, including: triple-zeta (cc-pvTZ) and quadruple-zeta (cc-pvQZ) basis sets [22]. These basis sets are very popular as the sets are large enough to minimize variational energy while simultaneously not being computationally expensive. Dunning's basis sets were developed for numerical efficiency in molecular calculations and therefore they are justified to use here. From here on, the 'cc-pv' will be dropped and the basis sets will be referred to as TZ and QZ.

For Density Functional Theory the B3LYP functional is used with the same basis sets [23]. The B3LYP functional is a "hybrid" functional, meaning it provides exact exchange energy in combination with correlation energy approximations. This functional is widely used for it's speed in calculations, having only 3 parameters, and it's common presence in literature.

4.2 Plume Dispersion

4.2.1 Gaussian Model

A Gaussian dispersion model is used to approximate the dispersion process. This model approximates dispersion as a point source H=300m from ground level where

a fire plume releases hydrogen cyanide at some constant rate Q given in units g/s. Since this work models stack height at ground level, height H is comprised solely of the initial plume rise resulting from the buoyancy arising due to heated air above the forest fire. There is also a constant wind coming from the west given in units m/s which contributes to the downstream (x-direction) evolution of the plume.

Turbulence parameters used include Pasquill D [20] for neutral wind conditions and open-country conditions σ_y and σ_z given by Briggs as [24]

$$\sigma_y(x) = 0.08x(1 + 0.0001x)^{-1/2} \tag{41}$$

and

$$\sigma_z(x) = 0.06x(1 + 0.0015x)^{-1/2} \tag{42}$$

where both equations are a function of x which is the downstream distance. Independently, σ_y and σ_z correspond to horizontal width and vertical extent of the downstream plume at a point given by x. For this work, x is assumed to be 2000 for the scenario of 2000m east of the source and zero for the case 2000m north.

Emission rate (g/s) of HCN was determined from a 2013 study of agricultural fires in the United States [6]. Emission factors (g/kg) were collected from 15 fires, measured from the NASA DC-8 aircraft. Fire number 5 was chosen to be modeled in this work due to a average field size and near-average emission factor (EF) $0.414g/kg$. The EF is defined as the mass of HCN released to mass of dry fuel consumed. The collection method for HCN is CF_3O^{-1}CIMS, chemical ionization mass spectrometry. The collection time for fire 5 is stated as 17:21-17:25, which is 4 minutes or 240 seconds. The emission rate Q is then defined as the ratio of the mass of HCN to the interval time of 240 seconds giving $Q = 0.002g/s$. It is assumed in this work that the single source concentration of HCN lies entirely on the centerline of the plume.

V. Results and Analysis

5.1 Spectroscopic Parameters

This section is a comparison between *ab initio* calculated spectroscopic parameters and experimentally determined literature values. The results are presented in alternating tables, where the first table displays Hartree-Fock calculations and the following table displays Density Functional Theory calculations. The first set of tables (in order) shows dipole moment (*debye*), bond lengths (*angstroms*), vibrationally dependent rotational constants (cm^{-1}), quartic and sextic centrifugal distortion constants (cm^{-1}), rovibrational partition functions, and anharmonic frequencies (cm^{-1}).

Table 1. Experimental vs. Theoretical dipole moment, bond lengths, vibration-rotation constants, rotational and centrifugal distortion constants, partition function, and anharmonic frequencies of $H^{12}C^{14}N$ calculated with Hartree-Fock method and the TZ and QZ basis sets

HCN	TZ	QZ	Experimental[a]
μ (*debye*)	3.263	3.262	2.985
r (CH) (Å)	1.0567	1.0569	1.0655
r (CN) (Å)	1.1244	1.1234	1.1532
B_v (cm^{-1})	1.5536	1.5558	1.4847
D_e (cm^{-1})	2.5730 x 10^{-6}	2.5797 x 10^{-6}	2.85 x 10^{-6}
H_e (cm^{-1})	2.9300 x 10^{-12}	2.9849 x 10^{-12}	2.7213 x 10^{-12}
Q_{vr}	137.34	137.17	149.94[b]
ω_1 (cm^{-1})	3615.9	3608.5	3442.5
ω_2	877.24	875.76	726.9
ω_3	2382.2	2407.2	2127.2

[a)]Ref.[16] [b)]Ref.[18]

Table 2. Experimental vs. Theoretical dipole moment, bond lengths, rotational and centrifugal distortion constants, partition function, and anharmonic frequencies of $H^{12}C^{14}N$ calculated with Density Functional (b3lyp) method and the TZ and QZ basis sets

HCN	TZ	QZ	Experimental[a]
μ $(debye)$	3.040	3.039	2.985
r (CH) (Å)	1.0543	1.0655	1.065
r (CN) (Å)	1.1507	1.1532	1.1532
B_v (cm^{-1})	1.5004	1.5024	1.4847
D_e (cm^{-1})	2.7617 x 10^{-6}	2.7702 x 10^{-6}	2.906 x 10^{-6}
H_e (cm^{-1})	2.5842 x 10^{-12}	2.6523 x 10^{-12}	2.7213 x 10^{-12}
Q_{vr}	145.53	145.34	149.94[b]
ω_1 (cm^{-1})	3446.3	2127.2	3442.5
ω_2	757.8	726.9	726.9
ω_3	2199.4	3442.5	2127.2

[a)]Ref.[18] [b)]Ref.[28]

The second set of tables follows the alternating table theme and shows (in order) transition dipole moments (*debye*) and fundamental vibrational modes (cm^{-1}).

Table 3. Experimental vs. Theoretical Transition Dipoles with Hartree-Fock method and TZ and QZ basis sets

HCN	TZ	QZ	Experimental[a]
$00^01 - 00^00$	0.0425	0.0420	0.001362[b]
$10^00 - 00^00$	0.0889	0.0887	0.0831[b]
ν_1 (cm^{-1})	2302.18	2384.62	2096.7
ν_2 (cm^{-1})	873.95	859.32	713.5
ν_3 (cm^{-1})	3564.33	3491.20	3442.5

[a)]Ref.[18] [b)]Ref.[28]

Table 4. Experimental vs. Theoretical Transition Dipoles with Density Functional (b3lyp) method and TZ and QZ basis sets

HCN	TZ	QZ	Experimental[a]
$00^01 - 00^00$	0.01546	0.01518	0.001362[b]
$10^00 - 00^00$	0.08676	0.08684	0.0831[b]
ν_1 (cm^{-1})	2172.9	2174.0	2096.7
ν_2 (cm^{-1})	746.6	746.6	713.5
ν_3 (cm^{-1})	3318.4	3314.6	3442.5

[a)]Ref.[18] [b)]Ref.[28]

5.2 Line Intensities

This section is a comparison between *ab initio* calculated line intensities and experimentally determined literature values from J=0 to J=29. Lorenztian fitted plots of the *ab initio* determined P and R branches follow each line intensity table, showing first the TZ results and then the QZ results. Both the tables and plots are given in terms of $cm^{-2}atm^{-1}$ at 298K. The first set of tables and plots give the line intensities for the CN stretch $00^01 - 00^00$ using Hartree-Fock and then using Density Functional Theory. The last set of tables and plots give the line intensities for the CH stretch $10^00 - 00^00$.

Table 5. Experimental vs. Theoretical Line Intensities ($cm^{-2}atm^{-1}$ at 298 K) for the $00^01 - 00^00$ band of $H^{12}C^{14}N$ calculated with Hartree-Fock and TZ and QZ basis sets

P Branch				R Branch		
Experimental[a]	QZ	TZ	J	TZ	QZ	Experimental[a]
-			0	0.32	0.32	1.93E-4
3.37E-4	0.93	0.95	1	0.95	0.93	3.00E-4
8.39E-4	1.50	1.53	2	1.54	1.51	2.95E-4
1.36E-3	2.01	2.05	3	2.07	2.02	2.36E-4
2.03E-3	2.42	2.48	4	2.51	2.45	1.71E-4
2.87E-3	2.75	2.80	5	2.85	2.78	7.25E-5
-	2.96	3.03	6	3.08	3.01	1.61E-5
4.23E-3	3.07	3.14	7	3.20	3.13	-
4.97E-3	3.08	3.15	8	3.22	3.15	2.97E-5
5.55E-3	3.00	3.07	9	3.15	3.08	1.24E-4
5.86E-3	2.85	2.92	10	3.00	2.93	2.22E-4
6.11E-3	2.64	2.70	11	2.79	2.72	3.58E-4
6.09E-3	2.40	2.45	12	2.53	2.48	5.06E-4
6.00E-3	2.13	2.18	13	2.25	2.20	6.70E-4
5.84E-3	1.85	1.89	14	1.96	1.92	7.96E-4
5.46E-3	1.57	1.61	15	1.68	1.64	9.10E-4
5.08E-3	1.32	1.35	16	1.41	1.37	1.00E-3
4.66E-3	1.08	1.11	17	1.16	1.13	-
4.06E-3	0.87	0.891	18	0.93	0.91	9.88E-4
3.51E-3	0.69	0.70	19	0.74	0.72	9.67E-4
2.97E-3	0.53	0.55	20	0.58	0.56	8.95E-4
2.49E-3	0.41	0.42	21	0.44	0.43	8.07E-4
1.95E-3	0.31	0.31	22	0.33	0.32	7.52E-4
1.61E-3	0.23	0.23	23	0.25	0.24	-
1.26E-3	0.16	0.17	24	0.18	0.17	4.90E-4
9.89E-4	0.12	0.12	25	0.13	0.13	4.09E-4
7.51E-4	0.08	0.08	26	0.09	0.09	-
5.70E-4	0.06	0.06	27	0.06	0.06	2.81E-4
4.06E-4	0.04	0.04	28	0.04	0.04	1.99E-4
2.97E-4	0.03	0.03	29	0.03	0.03	1.45E-4

[a)] Ref.[28]

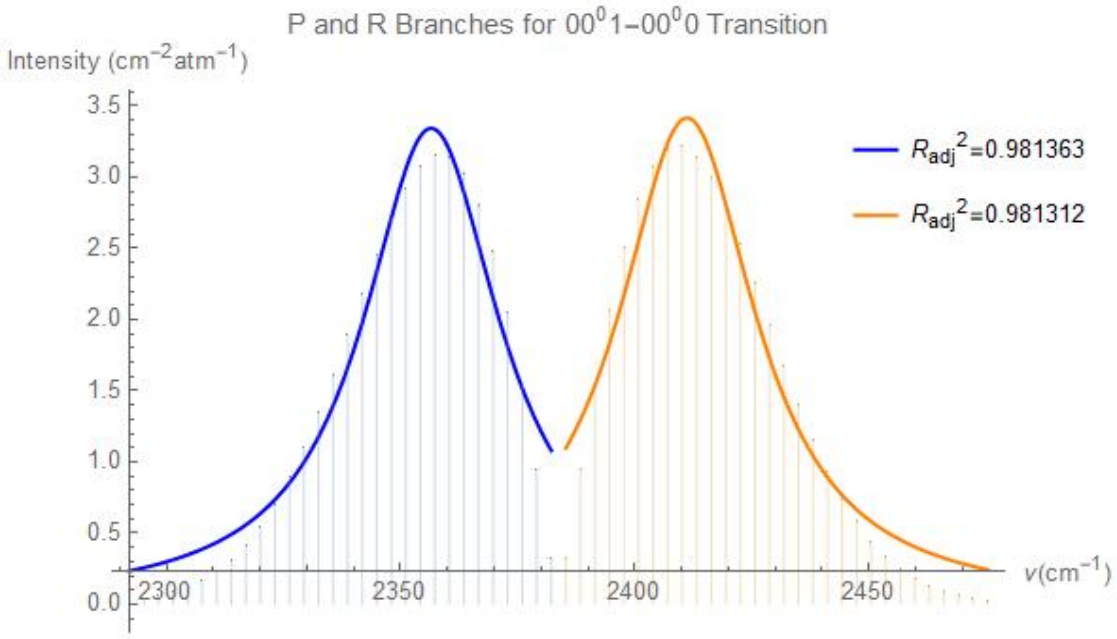

Figure 1. HF/TZ Calculated P and R branches for CN stretch fitted to a Lorentzian line shape. The intensities are shown in units of $cm^{-2}atm^{-1}$.

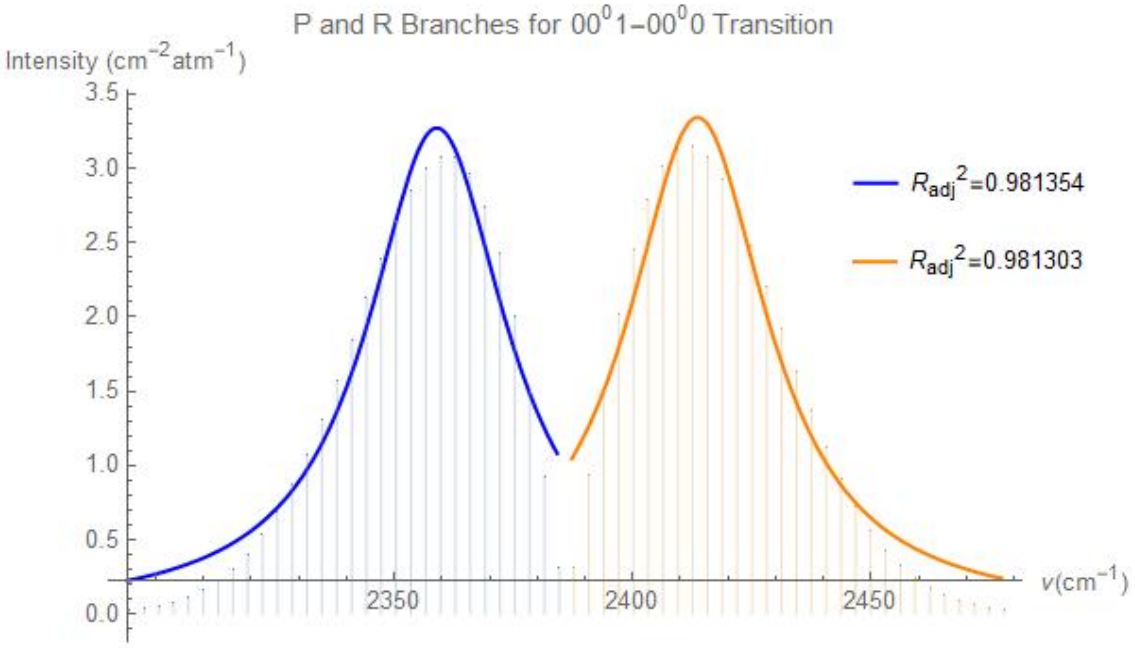

Figure 2. HF/QZ Calculated P and R branches for CN stretch fitted to a Lorentzian line shape. The intensities are shown in units of $cm^{-2}atm^{-1}$.

Table 6. Experimental vs. Theoretical line intensities ($cm^{-2}atm^{-1}$ at 298 K) for the 00^01-00^00 band of $H^{12}C^{14}N$ calculated with Density Functional (b3lyp) and TZ and QZ basis sets

P Branch				R Branch		
Experimental[a]	QZ	TZ	J	TZ	QZ	Experimental[a]
-			0	0.04	0.04	1.93E-4
3.37E-4	0.10	0.11	1	0.11	0.10	3.00E-4
8.39E-4	0.17	0.18	2	0.18	0.17	2.95E-4
1.36E-3	0.23	0.23	3	0.24	0.22	2.36E-4
2.03E-3	0.27	0.29	4	0.29	0.23	1.71E-4
2.87E-3	0.31	0.33	5	0.33	0.32	7.25E-5
-	0.34	0.35	6	0.36	0.34	1.61E-5
4.23E-3	0.35	0.37	7	0.378	0.360	-
4.97E-3	0.35	0.38	8	0.384	0.361	2.97E-5
5.55E-3	0.35	0.37	9	0.380	0.35	1.24E-4
5.86E-3	0.33	0.36	10	0.37	0.34	2.22E-4
6.11E-3	0.31	0.34	11	0.35	0.32	3.58E-4
6.09E-3	0.28	0.31	12	0.32	0.29	5.06E-4
6.00E-3	0.25	0.29	13	0.29	0.26	6.70E-4
5.84E-3	0.22	0.25	14	0.26	0.23	7.96E-4
5.46E-3	0.19	0.21	15	0.22	0.20	9.10E-4
5.08E-3	0.16	0.18	16	0.19	0.17	1.00E-3
4.66E-3	0.13	0.15	17	0.16	0.14	-
4.06E-3	0.11	0.13	18	0.13	0.11	9.88E-4
3.51E-3	0.09	0.10	19	0.11	0.09	9.67E-4
2.97E-3	0.07	0.08	20	0.09	0.07	8.95E-4
2.49E-3	0.05	0.06	21	0.07	0.05	8.07E-4
1.95E-3	0.04	0.05	22	0.05	0.04	7.52E-4
1.61E-3	0.03	0.04	23	0.04	0.03	-
1.26E-3	0.02	0.03	24	0.03	0.02	4.90E-4
9.89E-4	0.02	0.02	25	0.02	0.017	4.09E-4
7.51E-4	0.01	0.015	26	0.016	0.012	-
5.70E-4	0.008	0.01	27	0.012	0.008	2.81E-4
4.06E-4	0.005	0.008	28	0.008	0.006	1.99E-4
2.97E-4	0.004	0.005	29	0.006	0.004	1.45E-4

[a)] Ref.[28]

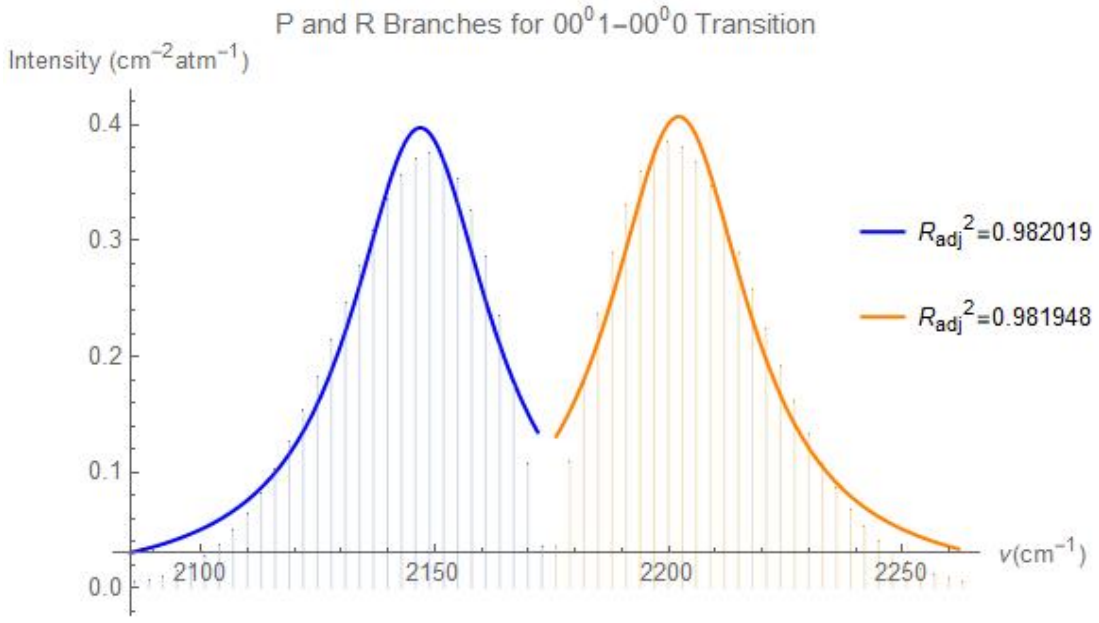

Figure 3. DFT B3LYP/TZ Calculated P and R branches for CN stretch fitted to a Lorentzian line shape. The intensities are shown in units of $cm^{-2}atm^{-1}$.

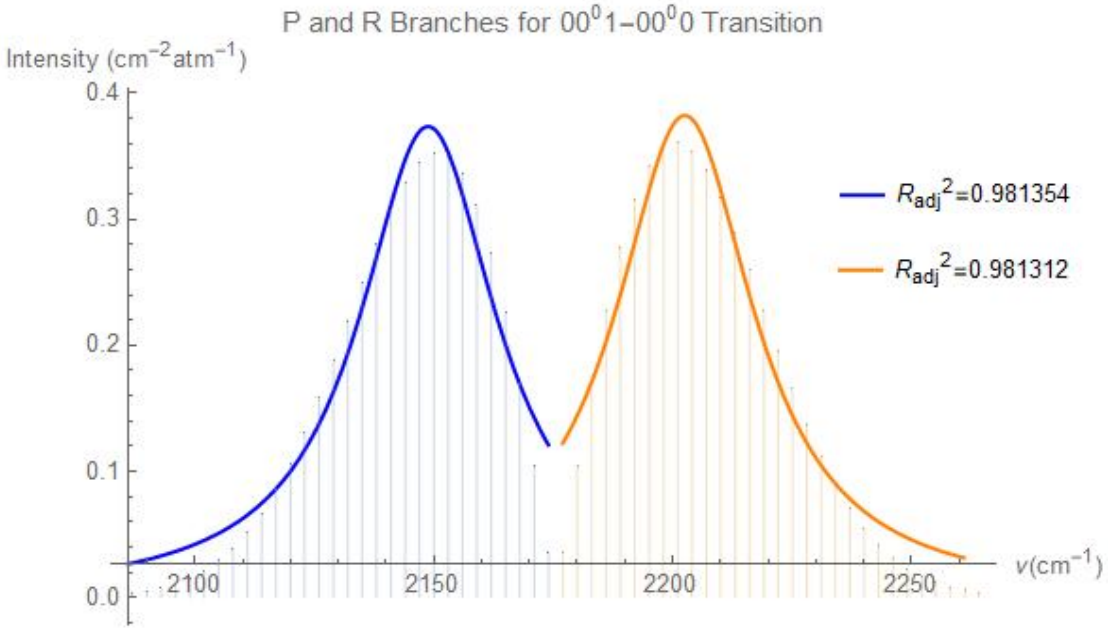

Figure 4. DFT B3LYP/QZ Calculated P and R branches for CN stretch fitted to a Lorentzian line shape. The intensities are shown in units of $cm^{-2}atm^{-1}$.

Table 7. Experimental vs. Theoretical line intensities ($cm^{-2}atm^{-1}$ at 298 K) for the $10^00 - 00^00$ band of $H^{12}C^{14}N$ calculated with Hartree-Fock and TZ and QZ basis sets

P Branch				R Branch		
Experimental[a]	QZ	TZ	J	TZ	QZ	Experimental[a]
-			0	2.062	2.055	1.601
1.574	6.064	6.083	1	6.099	6.080	3.165
3.086	9.798	9.829	2	9.873	9.841	4.593
4.450	13.10	13.14	3	13.23	13.18	5.854
5.610	15.85	15.90	4	16.03	15.97	6.898
6.541	17.95	18.01	5	18.19	18.12	7.699
7.216	19.36	19.43	6	19.66	19.59	8.226
7.642	20.09	20.17	7	20.44	20.36	8.536
7.809	20.17	20.25	8	20.56	20.48	8.487
7.741	19.67	19.75	9	20.09	20.01	8.260
7.460	18.687	18.77	10	19.12	19.04	7.854
7.021	17.33	17.41	11	17.77	17.69	7.297
6.467	15.71	15.79	12	16.15	16.07	6.630
5.822	13.94	14.02	13	14.36	14.28	5.901
5.147	12.12	12.19	14	12.51	12.44	5.162
4.470	10.33	10.39	15	10.68	10.62	4.408
3.716	8.639	8.691	16	8.950	8.896	3.726
3.140	7.089	7.135	17	7.360	5.902	2.517
2.559	5.711	5.750	18	5.943	5.902	2.517
2.081	4.519	5.750	19	4.713	4.679	2.018
1.638	3.514	4.552	20	3.672	3.644	1.591
1.284	2.685	3.541	21	2.812	2.789	1.229
0.989	2.016	2.707	22	2.117	2.099	0.936
0.747	1.489	2.034	23	1.566	1.552	0.704
0.555	1.081	1.502	24	1.140	1.129	0.519
0.406	0.772	1.091	25	0.816	0.807	0.382
0.293	0.542	0.780	26	0.574	0.568	0.269
0.207	0.374	0.548	27	0.398	0.393	0.190
0.145	0.254	0.379	28	0.271	0.268	0.129
0.099	0.170	0.257	29	0.181	0.179	0.088

[a)] Ref.[29]

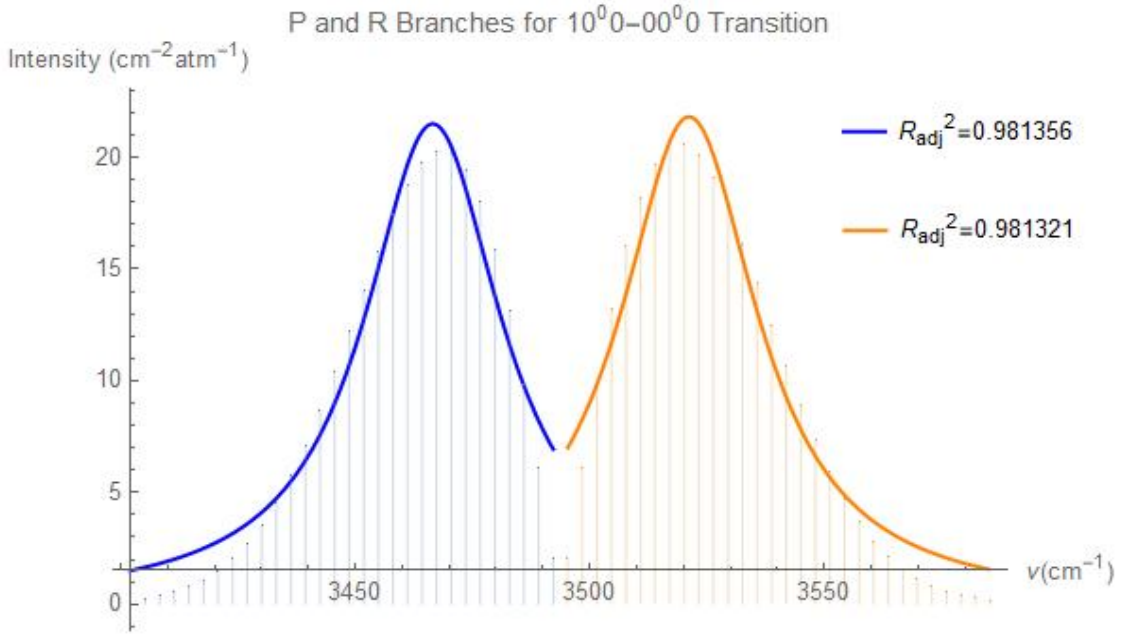

Figure 5. HF/TZ Calculated P and R branches for CH stretch fitted to a Lorentzian line shape. The intensities are shown in units of $cm^{-2}atm^{-1}$.

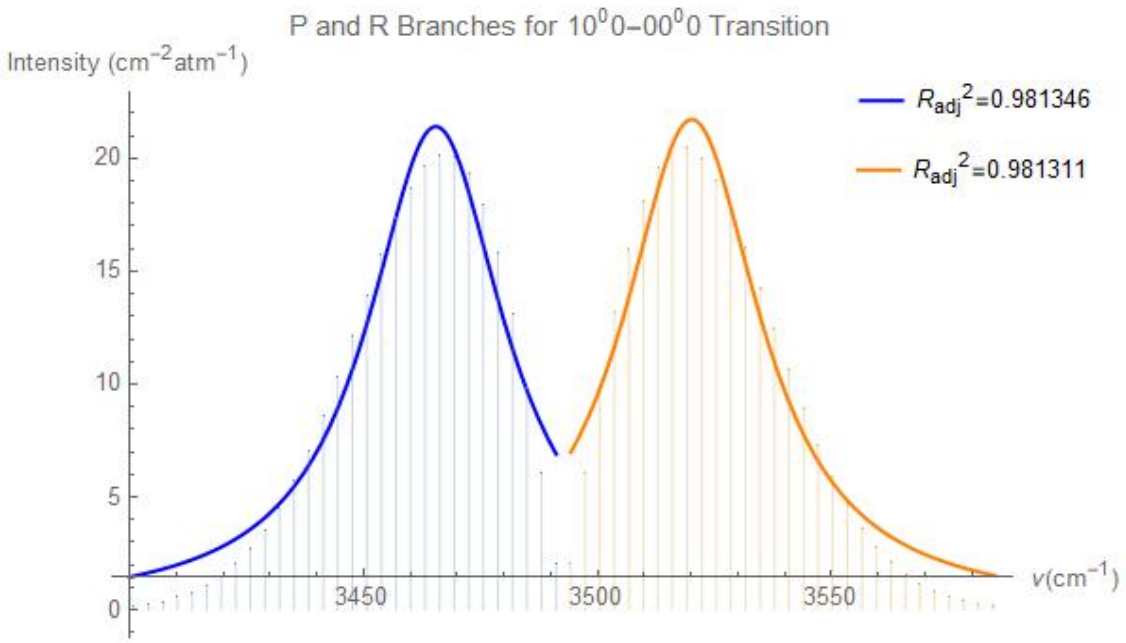

Figure 6. HF/QZ Calculated P and R branches for CH stretch fitted to a Lorentzian line shape. The intensities are shown in units of $cm^{-2}atm^{-1}$.

Table 8. Experimental vs. Theoretical line intensities ($cm^{-2}atm^{-1}$ at 298 K) for the 10^00-00^00 band of $H^{12}C^{14}N$ calculated with Density Functional (b3lyp) and TZ and QZ basis sets

P Branch				R Branch		
Experimental[a]	b3lyp/QZ	b3lyp/TZ	J	b3lyp/TZ	b3lyp/QZ	Experimental[a]
-			0	1.761	1.765	1.601
1.574	5.208	5.202	1	5.216	5.222	3.165
3.086	8.424	8.428	2	8.466	8.462	4.593
4.450	11.28	11.31	3	11.39	11.35	5.854
5.610	13.67	13.76	4	13.87	13.78	6.898
6.541	15.53	15.69	5	15.84	15.68	7.699
7.216	16.80	17.06	6	17.26	17.00	8.226
7.642	17.50	17.87	7	18.11	17.74	8.536
7.809	17.64	18.13	8	18.41	17.91	8.487
7.741	17.28	17.89	9	18.20	17.58	8.260
7.460	16.50	17.23	10	17.56	16.82	7.854
7.021	15.39	16.21	11	16.55	15.72	7.297
6.467	14.04	14.94	12	15.28	14.36	6.630
5.822	12.55	13.49	13	13.82	12.86	5.901
5.145	10.99	11.94	14	12.26	11.28	5.162
4.470	9.435	10.39	15	10.68	9.704	4.408
3.716	7.954	8.870	16	9.138	8.196	3.726
3.140	6.584	7.445	17	7.684	6.797	3.088
2.559	5.354	6.144	18	6.353	5.537	2.517
2.081	4.279	4.986	19	5.165	4.433	2.018
1.638	3.361	3.981	20	4.131	3.488	1.591
1.284	2.596	3.128	21	3.252	2.699	1.229
0.989	1.972	2.419	22	2.519	2.054	0.936
0.747	1.473	1.842	23	1.921	1.537	0.704
0.555	1.083	1.380	24	1.443	1.132	0.519
0.406	0.783	1.019	25	1.068	0.820	0.382
0.293	0.557	0.741	26	0.777	0.585	0.269
0.207	0.390	0.530	27	0.557	0.410	0.190
0.145	0.269	0.374	28	0.394	0.283	0.129
0.099	0.183	0.260	29	0.274	0.193	0.088

[a)] Ref.[29]

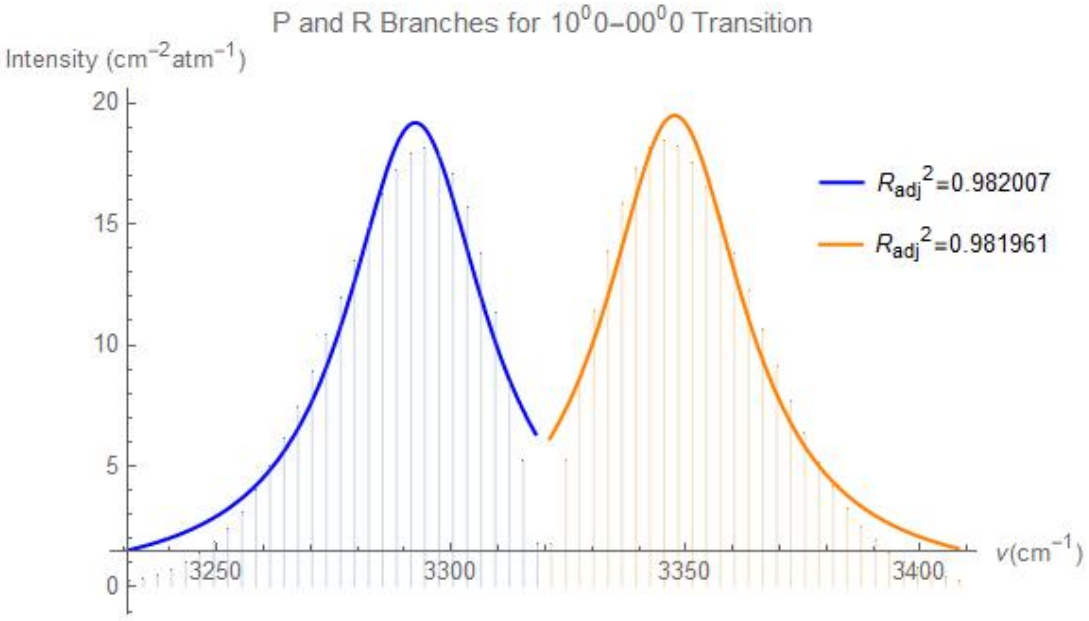

Figure 7. DFT B3LYP/TZ Calculated P and R branches for CH stretch fitted to a Lorentzian line shape. The intensities are shown in units of $cm^{-2}atm^{-1}$.

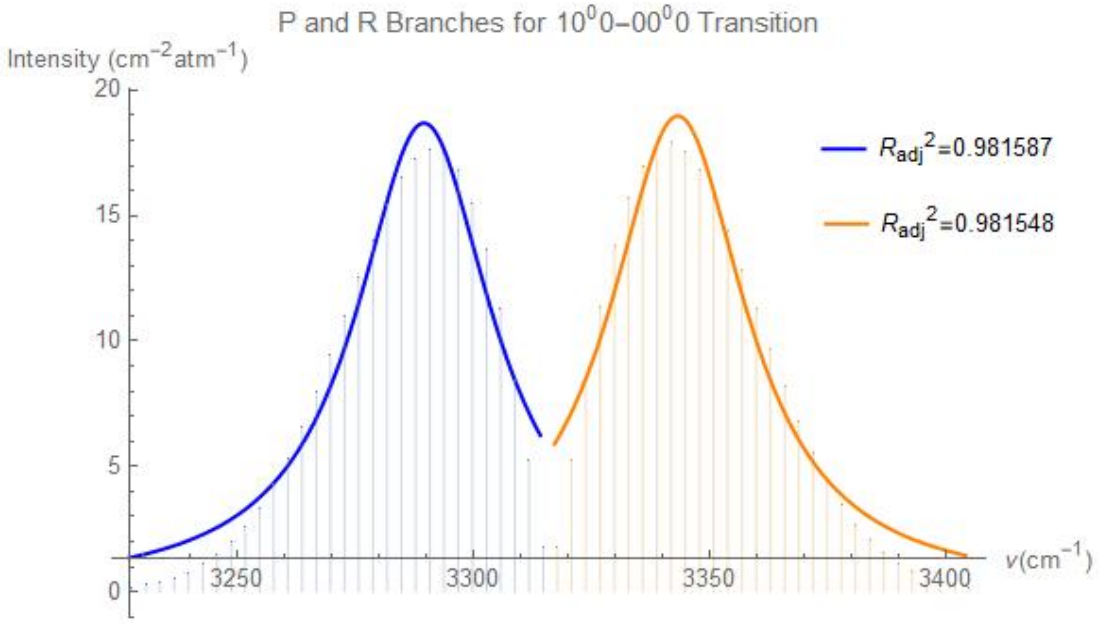

Figure 8. DFT B3LYP/QZ Calculated P and R branches for CH stretch fitted to a Lorentzian line shape. The intensities are shown in units of $cm^{-2}atm^{-1}$.

5.3 Plume Dispersion

To illustrate plume dispersion, an example is given using similar parameters of the intended link budget calculations, except with an altitude of $1000m$. The plume dispersion can for locations 2000m east and 2000m north of the point source can be seen in Figs. 9 and 10, respectively. We can see in Fig.9 the concentrations listed at the boundary layer of $1000m$ give on the right hand side. The actual altitude of interest is $100km$, which gives the concentration of $C = 5.46\text{x}10^{-7}\ g/m^3$.

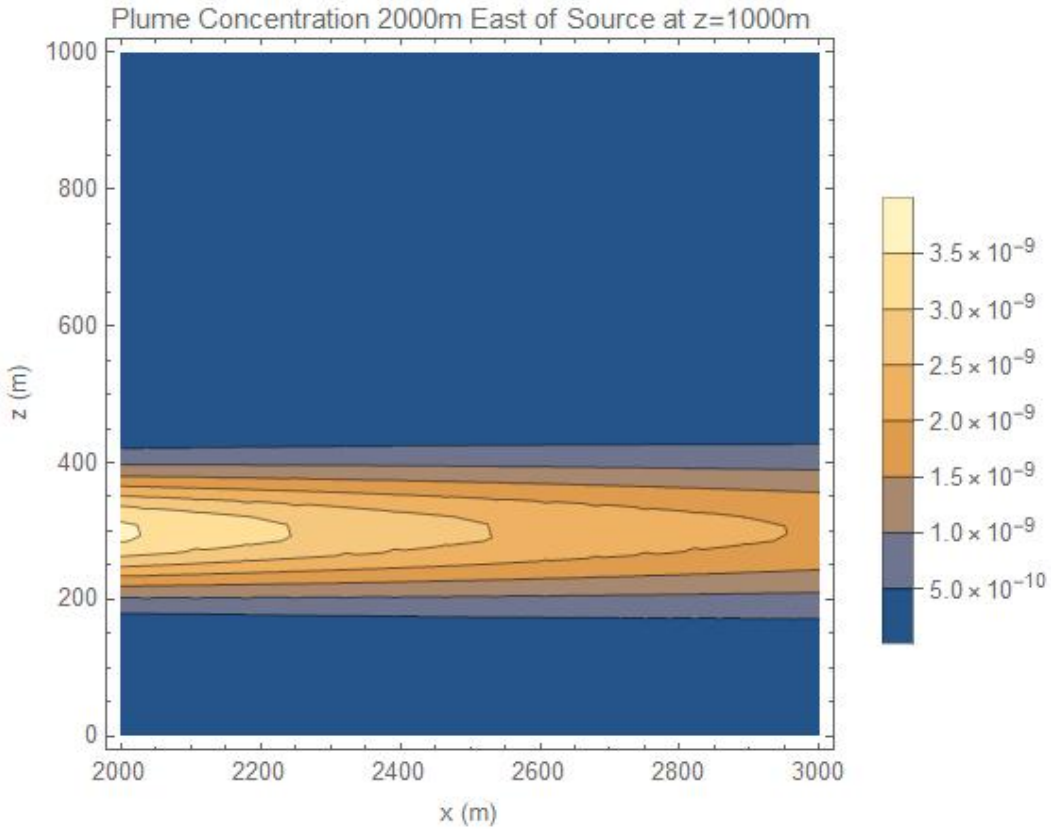

Figure 9. Plume concentration 2000m east of source at an altitude of 1000m. There is a 10 m/s wind speed coming from the west.

The calculations used in Figs. 9 and 10 approximate a point source located at coordinates (x,y,z)=(0,0,0). From Eqn.(37), we are defining the point source to have an emission rate $Q = 0.002g/s$, which was determined from emission factors of agricultural fires recorded in the United States [6]. In Fig. 9, we model the concentration

of the plume in g/m^3 with a downwind distance between 2000-3000m east of the source and an altitude of 1000m. The plot is intended to represent the dispersion of the plume in the case of a constant wind speed carrying the plume eastward.

In Fig.10 we use similar parameters for a location 2000m north of the point source. At the position, since the wind speed is only from the west, plume dispersion does not reach this location.

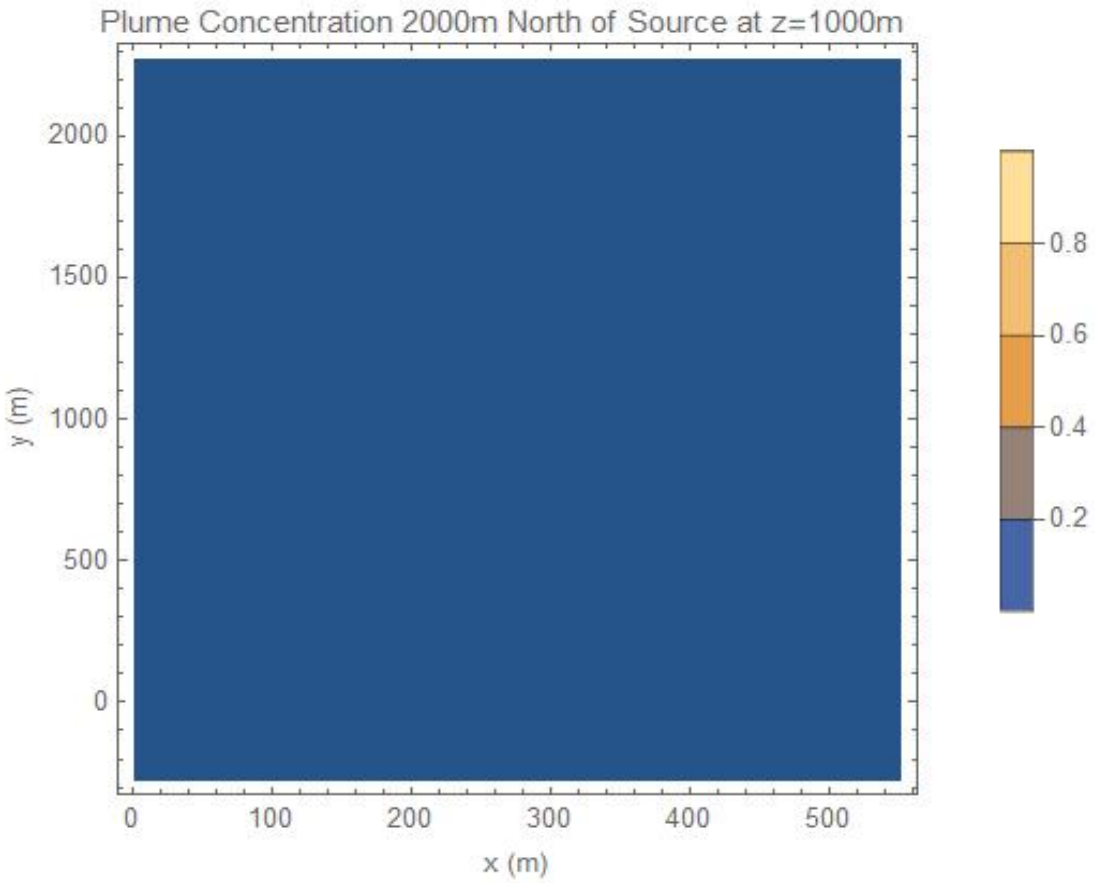

Figure 10. Plume concentration 2000m north of source at an altitude of 1000m. This location is not affected by the wind speed.

Determination of the value in the case of interest, an altitude of 100km, follows the same process of using Eqn.(37). As this altitude is quite large, numerical integration is used from ground=0 to z=100km at steps of 1m. For this case, a concentration of 5.463x10^{-7} g/m^3 was determined.

5.3.1 Total Attenuation: HCN Plume

Calculation of total attenuation of an HCN plume is determined in this section. The approach to calculating total attenuation was outlined in chapter 3, where the absorption coefficient ($cm^2 molecule^{-1}$) is determined from the product of spectral line intensity ($cm/molecule$) and the line shape used (cm). In this calculation, the HCN transition belonging to the V and W bands is the pure rotational $J_{1<-0}$ transition located at $2.956 cm^{-1}$ [25]. A similar line intensity equation to the ro-vibrational Eqn.(29) is given as [26]

$$S_{rot}(J) = \frac{11.183309(2B(J+1))}{Q_{rot}}(2J+1)e^{\frac{-BJ(J+1)}{kT}}(1-e^{\frac{-2B(J+1)}{kT}})\mathbf{M}_{J'J''} \tag{43}$$

where the previous ro-vibrational partition function Q_{vr} is replaced by rotational partition function Q_{rot}, the vibrational portion of the transition is removed, and the transition dipole $\mathbf{M}$ is only dependent on rotation. Since Eqn.(29) initially presented spectral line intensity in units of $cm^{-2}atm^{-1}$, a conversion factor is introduced [27] given by $cm^{-2}atm^{-1}$(1.3626 T x10^{-22}) $= cm/molecule$. Using the defined parameters for Eqn.(43), we get an HCN spectral line intensity for the $J_{1<-0}$ transition

$$S_{rot}(J_{1<-0}) = 3.97\text{x}10^{-22}(cm/molecule). \tag{44}$$

The product of the spectral line intensity and Lorentzian line shape function now gives the absorption coefficient as

$$k_{ij}(\nu, T) = 1.23\text{x}10^{-21}(cm^2 molecule^{-1}). \tag{45}$$

The plume concentration of HCN obtained was found in units of g/m^3. As we are interested in modeling HCN molecules a conversion is given

$$C = \frac{N}{V} = 5.46\text{x}10^{-7}\frac{g}{m^3} * \frac{1mol}{27.03g} * \frac{6.02\text{x}10^{23}molecules}{mol} * \frac{m^3}{1\text{x}10^6 cm} = 1.22\text{x}10^{10}\frac{molecules}{cm^2} \tag{46}$$

which gives us our concentration in units of $molecules$ of HCN per cm^2. The unitless optical depth can then be calculated by including the path length, $150km$, to our concentration giving

$$\tau_{ij}(\nu, T) = uk_{ij}(\nu, T) = (1.82\text{x}10^{18})(1.23\text{x}10^{-21}) = 0.00224. \tag{47}$$

Lastly, the attenuation in decibels (dB) for the HCN $J_{1<-0}$ transition is calculated as

$$A_{dB} = 10ln(e) = 4.343\tau = 0.00973(dB). \tag{48}$$

5.3.2 Link-Budget

We now have quantified a point source HCN plume's effect on signal attenuation 2000m east of the starting point with a wind speed blowing $10m/s$ out of the west. Returning to Eqn.(1) we can express the link budget 2000m east of the plume as

$$P_r = P_t - L_t - L_r - (0.00973dB) + G_t + G_r. \tag{49}$$

As there is no concentration of HCN 2000m north, the link budget is not effected.

VI. Discussion

6.1 Relevance of current Status

The current status of this work provides ab initio spectral line intensities and plume dispersion concentrations. The link between the two has been established allowing for the determination of attenuation due to Gaussian dispersion of a continuous point-source.

6.2 Future Work

6.2.1 Variable Wind Speed

It was assumed in our calculations that wind speed was a constant $10m/s$ coming out of the west. While this is fine for a simple model, wind speed should be modeled as a function of variable speed over time.

6.2.2 Bending Modes

The degenerate bending modes of hydrogen cyanide were not considered in this work. A similar methodology applies to these with slight variations in calculating the spectroscopic constants due to different selection rules for J transitions. Inclusion of these bending modes would allow for a complete picture of attenuation by HCN for a link budget, as there are degenerate bending modes at high J transitions within the V and W band region.

6.3 Conclusion

This work was able to establish a connection between *ab initio* calculations of spectroscopic parameters and molecular attenuation for a link budget. A good foundation

was set in order to obtain a complete profile of the role HCN plays in molecular attenuation. Our future work discussed further how this foundation can be strengthened and improved upon to reach the point of inclusion in a program such as LEEDR.

Bibliography

1. "Report ITU-R F.2323-0." Nov. 2015.

2. "IEEE 521-2002 - IEEE Standard Letter Designations for Radar-Frequency Bands." IEEE SA - The IEEE Standards Association - Home, 8 Jan. 2003, standards.ieee.org/standard/521-2002.html.

3. W/V-Band RF Propagation Experiment Design. ntrs.nasa.gov/api/citations/20120016067/downloads/20120016067.pdf?attachment=true.

4. Riva, C., et al. "The Challenge of Using the W Band in Satellite Communication." International Journal of Satellite Communications and Networking, vol. 32, no. 3, 2013, pp. 187–200., doi:10.1002/sat.1050.

5. Urbanski, Shawn P. "Chemical Composition of Wildland Fire Emissions." Developments in Environmental Science, vol. 8, 2009, doi:10.1016/S1474-8177(08)00004-1.

6. Liu, Xiaoxi, et al. "Agricultural Fires in the Southeastern U.S. during SEAC4RS: Emissions of Trace Gases and Particles and Evolution of Ozone, Reactive Nitrogen, and Organic Aerosol." Journal of Geophysical Research: Atmospheres, vol. 121, no. 12, 2016, pp. 7383–7414., doi:10.1002/2016jd025040.

7. Gilgallon, Paul F. "Modeling and Simulation of Scintillation and V/W Frequency Band." New York, Rome.

8. LEEDR Equations and Principles (LEAP). Air Force Institute of Technology, ENP, Center for Directed Energy, Aug. 2016.

9. I.E. Gordon, L.S. Rothman, C. Hill et al., "The HITRAN 2016 Molecular Spectroscopic Database", Journal of Quantitative Spectroscopy and Radiative Transfer. 203, 3-69 (2017)

10. Gaussian 16, Revision C.01, M. J. Frisch, G. W. Trucks, H. B. Schlegel, G. E. Scuseria, M. A. Robb, J. R. Cheeseman, G. Scalmani, V. Barone, G. A. Petersson, H. Nakatsuji, X. Li, M. Caricato, A. V. Marenich, J. Bloino, B. G. Janesko, R. Gomperts, B. Mennucci, H. P. Hratchian, J. V. Ortiz, A. F. Izmaylov, J. L. Sonnenberg, D. Williams-Young, F. Ding, F. Lipparini, F. Egidi, J. Goings, B. Peng, A. Petrone, T. Henderson, D. Ranasinghe, V. G. Zakrzewski, J. Gao, N. Rega, G. Zheng, W. Liang, M. Hada, M. Ehara, K. Toyota, R. Fukuda, J. Hasegawa, M. Ishida, T. Nakajima, Y. Honda, O. Kitao, H. Nakai, T. Vreven, K. Throssell, J. A. Montgomery, Jr., J. E. Peralta, F. Ogliaro, M. J. Bearpark, J. J. Heyd, E. N. Brothers, K. N. Kudin, V. N. Staroverov, T. A. Keith, R. Kobayashi, J. Normand, K. Raghavachari, A. P. Rendell, J. C. Burant, S. S. Iyengar, J. Tomasi, M. Cossi, J. M. Millam, M. Klene, C. Adamo, R. Cammi, J. W. Ochterski, R. L. Martin, K. Morokuma, O. Farkas, J. B. Foresman, and D. J. Fox, Gaussian, Inc., Wallingford CT, 2016.

11. "TECHNICAL ASPECTS OF PROTECTION FOR THE SCIENTIFIC USE OF THE 86 RADIO SPECTRUM." Handbook of Frequency Allocations and Spectrum Protection for Scientific Uses, The National Academies Press, 2015.

12. "The Link Budget and Fade Margin." Campbell Scientific, Inc., 2016.

13. "1.3 Interaction of Radiation with Matter." Spectra of Atoms and Molecules, by Peter F. Bernath, Third ed., Oxford University Press, 2020.

14. Clabo, D. Allen, et al. "A Systematic Study of Molecular Vibrational Anharmonicity and Vibration-Rotation Interaction by Self-Consistent-Field Higher-Derivative Methods. Asymmetric Top Molecules." Chemical Physics, vol. 123, 1988, pp. 187–239.

15. Clabo, D.A. Jr. “Systematic Studies of Molecular Vibrational Anharmonicity and Vibration-Rotation Interaction by Self-Consistent-Field Higher Derivative Methods: Applications to Asymmetric and Symmetric Top and Linear Polyatomic Molecules.” 1987, doi:10.2172/6117857.

16. Allen, Wesley D., et al. “A Systematic Study of Molecular Vibrational Anharmonicity and Vibration-Rotation Interaction by Self-Consistent-Field Higher-Derivative Methods. Linear Polyatomic Molecules.” Chemical Physics, vol. 145, 1990, pp. 427–466.

17. “6.2 Diatomic and Linear Molecules.” Spectra of Atoms and Molecules, by Peter F. Bernath, Third ed., Oxford University Press, 2020.

18. “7.8 Vibration-Rotation Line Intensities.” Spectra of Atoms and Molecules, by Peter F. Bernath, Third ed., Oxford University Press, 2020.

19. “Spectral Line Shape.” Wikipedia, Wikimedia Foundation, 14 Sept. 2020, en.wikipedia.org/wiki/Spectral-line-shape

20. “4. Gaussian Plume Model for Continuous Sources.” Handbook on Atmospheric Diffusion, by Steven R. Hanna et al., Technical Information Center, U.S. Dept. of Energy, 1982.

21. “2. Table of Physical Quantities.” Quantities, Units and Symbols in Physical Chemistry, Second ed., Blackwell Science Ltd., 1993, pp. 31–32.

22. “Basis Sets.” Gaussian.com, gaussian.com/basissets/.

23. “1. What Is Density Functional Theory?” Density Functional Theory: a Practical Introduction, by David Sholl et al., Wiley, 2011.

24. Briggs, G A. Diffusion estimation for small emissions. Preliminary report. United States: N. p., 1973. Web. doi:10.2172/5118833.

25. HCN Spectral Data, physics.nist.gov/cgi-bin/MolSpec/trisearch

26. Harris, Gregory John. "An Ab Initio HCN/HNC Rotational-Vibrational Line List and Opacity Function for Astronomy." University of London, ProQuest LLC, 2015.

27. Pugh, Larry A., and K. Narahari Rao. "Chapter 4 Intensities From Infrared Spectra." Molecular Spectroscopy: Modern Research, II, Academic Press Inc. (London) Ltd., 1976, pp. 170–171.

28. Maki, Arthur, et al. "The CN Mode of HCN: A Comparative Study of the Variation of the Transition Dipole and Herman–Wallis Constants for Seven Isotopomers and the Influence of Vibration–Rotation Interaction." Journal of Molecular Spectroscopy, vol. 174, no. 2, 1995, pp. 365–378., doi:10.1006/jmsp.1995.0008.

29. Malathy Devi, V, et al. "A Multispectrum Analysis of the 1 Band of H12C14N: Part I. Intensities, Self-Broadening and Self-Shift Coefficients." Journal of Quantitative Spectroscopy and Radiative Transfer, vol. 82, no. 1-4, 2003, pp. 319–341., doi:10.1016/s0022-4073(03)00161-4.

REPORT DOCUMENTATION PAGE

Form Approved
OMB No. 0704–0188

1. REPORT DATE *(DD–MM–YYYY)*	2. REPORT TYPE	3. DATES COVERED *(From — To)*
03–08–2021	Master's Thesis	Sept 2020 — Mar 2021

4. TITLE AND SUBTITLE

Ab Initio Spectroscopy of Natural and Artificial Fire Contaminants for Microwave Frequency (V/W Band) Signal Absorbance

5a. CONTRACT NUMBER

5b. GRANT NUMBER

5c. PROGRAM ELEMENT NUMBER

6. AUTHOR(S)

Husk, Matthew B.

5d. PROJECT NUMBER

5e. TASK NUMBER

5f. WORK UNIT NUMBER

7. PERFORMING ORGANIZATION NAME(S) AND ADDRESS(ES)

Air Force Institute of Technology
Graduate School of Engineering an Management (AFIT/EN)
2950 Hobson Way
WPAFB OH 45433-7765

8. PERFORMING ORGANIZATION REPORT NUMBER

AFIT-ENG-MS-18-D-001

9. SPONSORING / MONITORING AGENCY NAME(S) AND ADDRESS(ES)

Air Force Research Laboratory/RIT
Paul F. Gilgallon, Principal Engineer, NC3 Systems and Technology Lead
525 Brooks Road
Rome, NY 13441.

10. SPONSOR/MONITOR'S ACRONYM(S)

AFRL/RIT

11. SPONSOR/MONITOR'S REPORT NUMBER(S)

12. DISTRIBUTION / AVAILABILITY STATEMENT

DISTRIBUTION STATEMENT A:
APPROVED FOR PUBLIC RELEASE; DISTRIBUTION UNLIMITED.

13. SUPPLEMENTARY NOTES

14. ABSTRACT

The rotation and vibration spectral properties including frequencies and intensities for highly concentrated molecules present in wildland and artificial fires have been studied. Properties were used to determine absorption and its effect in a link budget analysis. Absorption in link budget analyses is commonly accounted for via line-by-line methodology aided by HITRAN documented intensities. Limited, if any, customization of spectral properties is available with HITRAN and other spectral databases. *Ab initio* quantum chemistry calculations with Dunning's correlation consistent triple and quadruple-zeta atomic basis sets were employed to obtain structures, dipole moments, rotational-vibrational frequencies and intensities, as well as various coupling parameters. Anharmonic corrections to the vibrational energies are included in the calculations. The values of these parameters were found to be in agreement with experimental data while allowing flexibility for the inclusion or exclusion of spectral properties for various gases. Discussed here is molecular absorption in relation to a link budget, an overview of vibration-rotation constants for various molecular geometries, a description of intensities calculated from transition dipole, and lastly power-loss due to absorption.

15. SUBJECT TERMS

Ab Initio, Rotational Spectroscopy, Rotational-Vibrational Spectroscopy, Microwave, Molecular Attenuation, V Band, W Band

16. SECURITY CLASSIFICATION OF:			17. LIMITATION OF ABSTRACT	18. NUMBER OF PAGES	19a. NAME OF RESPONSIBLE PERSON
a. REPORT	b. ABSTRACT	c. THIS PAGE			19b. TELEPHONE NUMBER *(include area code)*
U	U	U	UU	59	